

Research Report

A continuum-based analytical approach to evaluate response of single piles under dynamic lateral loading

Submitted to

Mid-Atlantic Universities Transportation Center

and

Larson Transportation Institute

The Pennsylvania State University, University Park

Nina Zabihi
Dr. Prasenjit Basu
Dr. Swagata B. Basu

September 2014

Table of Contents

Abstract.....	3
Introduction.....	4
Problem definition	5
Displacement and strain fields	6
Governing differential equations.....	8
Solution algorithm.....	12
Solution for a specific case – undamped pile-soil system under steady state harmonic loading..	14
Analytical Solution for Pile Deflection.....	15
Finite Difference Formulation for Soil Displacement Shape Functions.....	17
Results and Discussions	20
Summary and Conclusions	29
References.....	30

Abstract

The pressing need for building resilient and sustainable civil infrastructure systems requires optimal design of infrastructure components which are not only capable to perform adequately under service loads but also resilient enough to survive under loads from man-made and natural extreme events. This report focuses on a component of seismic fragility analysis of bridge foundations – load-displacement behavior of piles under dynamic lateral loading. Winkler (soil-spring) models are widely used to capture pile-soil interaction under lateral loading. However, such simplified foundation-soil interaction model cannot predict ‘true’ serviceability and limit conditions. Consequently, a high level of conservatism is employed in such analyses, and therefore simplified soil spring models cannot be relied upon in the assessment of reliability (or vulnerability) of bridge foundations under dynamic loading.

In order to effectively capture different possible damage conditions in foundations and their complex interaction with structures, a continuum-based analytical framework is explored in this study to investigate behavior of single piles under dynamic lateral loading. The governing differential equations for the pile-soil system are derived by using Hamilton’s principle. The soil displacement field is assumed to be consistent with two facts: (i) soil displacement decreases as the distance from the pile increases and (ii) in addition to the radial distance from pile, soil displacement at any point depends on the direction of the load with respect to that point. Because of the interdependency between pile deflection and soil displacement, an iterative solution scheme is adopted. The adopted analysis framework shows promise to eliminate the need for computationally expensive numerical analyses (e.g., 3D finite element analysis). It is anticipated that future research based on the work presented in this report will facilitate generation of pile fragility curves that can provide probabilistic estimation of foundation vulnerability under dynamic loading.

Introduction

Piles are often used as foundation elements for structures subjected to both axial and lateral loads. In situations when structures are exposed to high lateral load demands (such as due to machine vibrations, seismic motions, extreme wind load, sea waves, to name a few) response of pile foundations under static and/or dynamic lateral load should be critically investigated to avoid any catastrophic structural failure initiated by the failure of foundations.

Over the last few decades, different analytical and numerical approaches have been adapted to model and analyze pile-soil interaction and dynamic response of pile foundations. Winkler spring-based models are the simplest among all available models. In such models, soil continuum and piles are, respectively, approximated as discretely-spaced and interconnected springs. In some variations of such discrete modeling approach, dashpots are also connected to one or more pile segments. The spring and dashpot constants are either back-calculated from experimental data or directly fed in to the models based on analytical considerations and judgement. The Novak model (Novak 1974) and the Matlock model (Matlock et al. 1978) are known as the conventional Winkler models that are frequently used in dynamic response analysis of pile foundations. The Nogami model (Nogami et al. 1988; 1991) is another variation of spring-based model that can account for nonlinear pile-soil interaction under dynamic loading. Other researchers also attempted to account for nonlinearity and inhomogeneity in the soil continuum, pile-soil separation and hysteretic degradation of soil through modified versions of Winkler model. For example, El Naggar and Bentley (2000) and Maheshwari and Watanaba (2006) used nonlinear springs to take into account the gapping at the soil-pile interface. Numerical simplicity and the ease of implementation are among the top advantages of Winkler models; however, such models are not capable of (i) considering shear transfer within soil (i.e., shear interaction between two adjacent layers of soil) and (2) capturing the three-dimensional interaction between the pile and the soil. Such shortcomings of Winkler models can be overcome by using continuum-based methods.

Continuum-based approaches for analyzing pile-soil interaction under lateral loading can broadly be divided into two categories: using numerical techniques (e.g., finite element, finite difference) and using analytical or semi-analytical techniques. Finite element method has extensively been used by researchers for analysis of laterally loaded piles (Kuhlemar 1979, Krishna et al. 1983, Velez et al. 1983). In finite element analyses of piles under dynamic lateral

loading, the far field is represented by energy-absorbing boundaries. More advanced finite element analyses consider the effects of soil plasticity and separation at pile-soil interface on dynamic lateral response of piles (e.g. Bentley and El Naggar 2000, and Maheshwari et al. 2004). In spite of their superior capability in analyzing soil-pile interaction, three-dimensional numerical analyses are computationally expensive for routine practices. Therefore, analytical or semi-analytical methods are more appealing.

Considering the soil surrounding the pile as a linear elastic continuum, Das et al. 1999 developed analytical solutions to obtain lateral pile deflection along the length of the pile. However, they assumed the same decreasing trend of soil displacement in both the radial and tangential directions with the increase of distance from the pile. In case of single pile under static lateral loading, Basu et al. 2009 indicated that the consideration of the same decreasing trend of soil displacement in both radial and tangential directions would result in a soil response stiffer than that is in reality.

The present study explores a continuum-based, semi-analytical framework for dynamic analysis of laterally loaded single piles. Pile and soil displacements under simultaneous actions of dynamic lateral load $F(t)$ and moment $M(t)$ are quantified as a function of depth and time. The analytical formulation is based on the facts that soil displacement decreases as the distance from the pile increases and displacement at any point in the soil surrounding the pile depends on the direction of applied load with respect to the point of interest. Hamilton's principle is utilized in deriving the governing differential equations that describe pile and soil displacements. Appropriate boundary conditions are enforced to obtain simultaneous solution for pile and soil displacements. For a specific case of steady state harmonic loading, closed-form solution is obtained for pile deflection. Soil displacement fields are evaluated using one-dimensional finite difference technique.

Problem definition

We consider a circular pile with length L_p and radius r_p embedded in a semi-infinite, homogeneous, isotropic soil deposit. The pile head is subjected to a time dependent lateral force $F(t)$, and a time dependent moment $M(t)$, such that $F(t)$ and $M(t)$ are orthogonal vectors (Fig. 1). The cylindrical coordinate system (r, θ, z) is employed with its origin at the center of the pile

head and the positive z axis (which coincides with the pile axis) pointing downwards. Specific assumptions made in the present analysis are:

- i. constitutive behavior of soil is elastic with shear modulus G_s and Lamé's constant λ_s
- ii. the pile is vertical and it behaves as an Euler-Bernouli beam with a constant flexural rigidity $E_p I_p$ throughout its length; E_p and I_p are, respectively, the Young's modulus of pile material and second moment of inertia for pile cross section
- iii. the pile is perfectly connected to the soil; i.e. there is no separation or slippage at the pile and soil interface
- iv. vertical displacement of the pile under the lateral load and moment is negligible.
- v. time-dependent pile displacement is a function of depth z only; i.e., displacement at every point on a pile cross section at depth z is constant

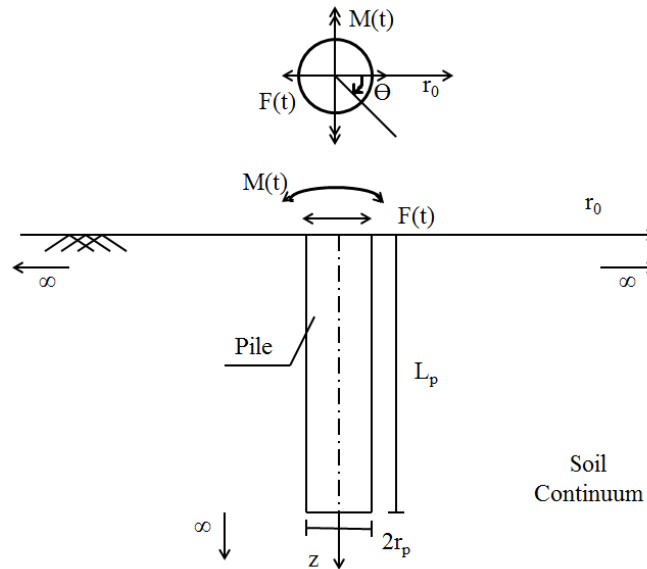


Figure 1 Problem geometry – single pile under dynamic lateral loading

Displacement and strain fields

Displacement of any point at depth z within the ground is assumed to be a function of radial pile displacement $w(z, t)$ at the same depth (Fig. 2). Dimensionless displacement shape functions $\phi_r(r)$ and $\phi_\theta(r)$ are used to account for the decay in soil displacement with increase in radial distance away from the pile. $\phi_r(r)$ and $\phi_\theta(r)$ are equal to 1 at $r = r_p$ (compatibility at pile and soil interface) and are equal to 0 at $r \rightarrow \infty$. For the domain below the pile (i.e., for $z > L_p$),

$w(z, t)$ is the displacement of the soil column, with radius r_p and extending infinitely below the pile. Displacement components at any point within the soil domain are expressed as:

$$u_r(r, \theta, z, t) = w(z, t)\phi_r(r) \cos \theta \quad (1a)$$

$$u_\theta(r, \theta, z, t) = -w(z, t)\phi_\theta(r) \sin \theta \quad (1b)$$

$$u_z(z, t, r, \theta) = 0 \quad (1c)$$

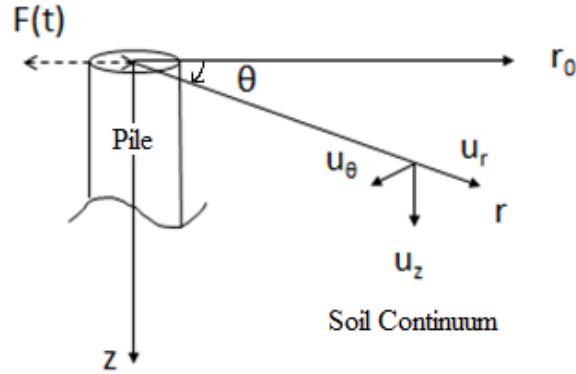


Figure 2 Soil displacement components at a point within the ground

The strain components at any point within the ground are derived following the displacement components described in equation (1).

$$\begin{bmatrix} \epsilon_{rr} \\ \epsilon_{\theta\theta} \\ \epsilon_{zz} \\ \gamma_{r\theta} \\ \gamma_{rz} \\ \gamma_{\theta z} \end{bmatrix} = \begin{bmatrix} -\frac{\partial u_r}{\partial r} \\ -\frac{u_r}{r} - \frac{1}{r} \frac{\partial u_\theta}{\partial \theta} \\ -\frac{\partial u_z}{\partial z} \\ \frac{u_\theta}{r} - \frac{1}{r} \frac{\partial u_r}{\partial \theta} - \frac{\partial u_\theta}{\partial r} \\ -\frac{u_z}{r} - \frac{\partial u_r}{\partial z} \\ -\frac{u_\theta}{z} - \frac{1}{r} \frac{\partial u_z}{\partial \theta} \end{bmatrix} = \begin{bmatrix} -w(z) \frac{d\phi_r(r)}{dr} \cos \theta \\ -w(z) \frac{\phi_r(r) - \phi_\theta(r)}{r} \cos \theta \\ 0 \\ w(z) \left\{ \frac{\phi_r(r) - \phi_\theta(r)}{r} - \frac{d\phi_r(r)}{dr} \right\} \sin \theta \\ -\frac{dw(z)}{dz} \phi_r(r) \cos \theta \\ \frac{dw(z)}{dz} \phi_\theta(r) \sin \theta \end{bmatrix} \quad (2)$$

Governing differential equations

The governing differential equations for pile deflection and soil displacement are obtained following the Hamilton's principle for deformable bodies. Mathematically,

$$\int_{t_1}^{t_2} (\delta W_{nc} + \delta T - \delta U) dt = 0 \quad (3)$$

where W_{nc} is work done by non-conservative forces, T and U are respectively, kinetic and potential energy associated with the pile-soil system. The operator δ is used to signify variation of a physical quantity. The potential energy U of the pile and soil system is given by:

$$\begin{aligned} U = & \frac{1}{2} \int_0^L E_p I_p \left(\frac{\partial^2 w}{\partial z^2} \right)^2 dz + \frac{1}{2} \int_{r_p}^{\infty} \int_0^{2\pi} \int_0^{L_p} (\sigma_{rr} \epsilon_{rr} + \sigma_{\theta\theta} \epsilon_{\theta\theta} + \tau_{r\theta} \gamma_{r\theta} + \tau_{rz} \gamma_{rz} + \\ & \tau_{\theta z} \gamma_{\theta z}) r dr d\theta dz + \frac{1}{2} \int_0^{\infty} \int_0^{2\pi} \int_{L_p}^{\infty} (\sigma_{rr} \epsilon_{rr} + \sigma_{\theta\theta} \epsilon_{\theta\theta} + \tau_{r\theta} \gamma_{r\theta} + \tau_{rz} \gamma_{rz} + \\ & \tau_{\theta z} \gamma_{\theta z}) r dr d\theta dz \end{aligned} \quad (4)$$

Combining equations (2) and (4), the potential energy of the pile-soil system can be rewritten as:

$$\begin{aligned} U = & \frac{1}{2} E_p I_p \int_0^L \left(\frac{\partial^2 w}{\partial z^2} \right)^2 dz + \frac{\pi}{2} \int_0^{\infty} \int_{r_p}^{\infty} \{ (\lambda_s + 2G_s) w^2 \left(\frac{d\phi_r}{dr} \right)^2 + 2\lambda_s w^2 \frac{d\phi_r}{dr} \frac{(\phi_r - \phi_{\theta})}{r} + \\ & (\lambda_s + 3G_s) w^2 \frac{(\phi_r - \phi_{\theta})^2}{r^2} + G_s w^2 \left(\frac{d\phi_{\theta}}{dr} \right)^2 + 2G_s w^2 \frac{d\phi_{\theta}}{dr} \frac{(\phi_r - \phi_{\theta})}{r} + G_s \left(\frac{dw}{dz} \right)^2 \phi_r^2 + \\ & G_s \left(\frac{dw}{dz} \right)^2 \phi_{\theta}^2 \} r dr dz + \frac{\pi}{2} r_p^2 \int_{L_p}^{\infty} G_s \left(\frac{dw}{dz} \right)^2 dz \end{aligned} \quad (5)$$

The kinetic energy T of the pile and soil system is:

$$\begin{aligned} T = & \frac{1}{2} \int_0^{L_p} \rho_p A_p \left(\frac{\partial w}{\partial t} \right)^2 dz + \frac{1}{2} \int_{L_p}^{\infty} \rho_s A_p \left(\frac{\partial w}{\partial t} \right)^2 dz + \frac{1}{2} \int_0^{2\pi} \int_{r_p}^{\infty} \int_0^{\infty} \rho_s \left\{ \left(\frac{\partial u_r}{\partial t} \right)^2 + \right. \\ & \left. \left(\frac{\partial u_{\theta}}{\partial t} \right)^2 \right\} r dz dr d\theta \end{aligned} \quad (6)$$

where ρ_p and ρ_s are density of the pile materials and soil, respectively, and A_p is cross section area of the pile. Using equation (1) in (6), kinetic energy T for the pile-soil system can be rewritten as:

$$T = \frac{1}{2} \rho_p A_p \int_0^{L_p} \left(\frac{\partial w}{\partial t}\right)^2 dz + \frac{1}{2} \rho_s A_p \int_{L_p}^{\infty} \left(\frac{\partial w}{\partial t}\right)^2 dz + \frac{\pi}{2} \rho_s \int_0^{\infty} \int_{r_p}^{\infty} \left\{ \left(\frac{\partial w}{\partial t}\right)^2 \phi_r^2 + \left(\frac{\partial w}{\partial t}\right)^2 \phi_{\theta}^2 \right\} r dr dz \quad (7)$$

Now, the work done by the non-conservative forces in variational form can be expressed as:

$$\delta W_{nc} = -F(t) \cdot \delta w(0, t) + M(t) \frac{\partial \delta w(0, t)}{\partial z} + \int_0^{\infty} c \frac{\partial w}{\partial t} \delta w dz \quad (8)$$

where, c represents damping of the pile-soil system. Combining equations (3), (5), (7), and (8) and applying principles of variational calculus:

$$\int_{t_1}^{t_2} (\delta W_{nc} + \delta T - \delta U) dt = \int_{t_1}^{t_2} \{ [A(w) \delta w + B(w) \delta \left(\frac{dw}{dz}\right)] + [C(\phi_r) \delta \phi_r] + [D(\phi_{\theta}) \delta \phi_{\theta}] \} dt = 0 \quad (9)$$

The terms associated with each of the variations δw , $\delta \left(\frac{dw}{dz}\right)$, $\delta \phi_r$, and $\delta \phi_{\theta}$ must individually be equal to zero to satisfy equation (9). This exercise yields the governing differential equations and boundary conditions needed for solving $w(z, t)$, $\phi_r(r)$, and $\phi_{\theta}(r)$.

Collecting the coefficients of δw and $\delta \left(\frac{dw}{dz}\right)$ for the domains $0 \leq z \leq L_p$ and $L_p \leq z$ and equating each to zero yields the differential equations and boundary conditions that govern the radial deflections of the pile and the soil column (extending infinitely) below the pile.

- *Differential equations*

$$E_p I_p \frac{\partial^4 w}{\partial z^4} - 2\tau \frac{\partial^2 w}{\partial z^2} + kw + M_1 \frac{\partial^2 w}{\partial t^2} + c \frac{\partial w}{\partial t} = 0 \quad \text{for } 0 \leq z \leq L_p \quad (10)$$

$$-2\tau_s \frac{\partial^2 w}{\partial z^2} + kw + M_2 \frac{\partial^2 w}{\partial t^2} + c \frac{\partial w}{\partial t} = 0 \quad \text{for } z \geq L_p \quad (11)$$

- *Boundary conditions*

At the ground surface (i.e. $z = 0$):

$$E_p I_p \frac{\partial^3 w}{\partial z^3} - 2\tau \frac{\partial w}{\partial z} = F \quad (12a)$$

$$E_p I_p \frac{\partial^2 w}{\partial z^2} = M \quad (12b)$$

At the bottom of the pile (i.e. $z = L_p$):

$$E_p I_p \frac{\partial^3 w}{\partial z^3} - 2\tau \frac{\partial w}{\partial z} = -2\tau_s \frac{\partial w_{\text{in soil}}}{\partial z} \quad (13a)$$

$$E_p I_p \frac{\partial^2 w}{\partial z^2} = 0 \quad (13b)$$

Pile-soil interface at $z = L_p$:

$$w_{\text{in pile}} = w_{\text{in soil}} \quad (14a)$$

At $z \rightarrow \infty$ (i.e., at a distance far below the pile base):

$$w = 0 \quad (14b)$$

Parameters M_1 , M_2 , τ , τ_s , and k in equations (10) through (13) are defined as:

$$M_1 = \rho_p A_p + \pi \rho_s \int_{r_p}^{\infty} r (\phi_r^2 + \phi_\theta^2) dr \quad (15a)$$

$$M_2 = \rho_s A_p + \pi \rho_s \int_{r_p}^{\infty} r (\phi_r^2 + \phi_\theta^2) dr \quad (15b)$$

$$2\tau = \pi G \int_{r_p}^{\infty} r (\phi_r^2 + \phi_\theta^2) dr \quad (15c)$$

$$2\tau_s = 2\tau + \pi G r_p^2 \quad (15d)$$

$$k = \pi [(\lambda + 2G)\eta_1 + G\eta_2 + 2\lambda\eta_3 - 2G\eta_4 - 2\lambda\eta_5 + 2G\eta_6 + (\lambda + 3G)\eta_7 + (\lambda + 3G)\eta_8 - 2(\lambda + 3G)\eta_9] \quad (15e)$$

The η terms in equation (15c) are functions of displacement shape functions and their derivatives.

$$\begin{aligned}
\eta_1 &= \int_{r_p}^{\infty} \left(\frac{d\phi_r}{dr} \right)^2 r dr & \eta_2 &= \int_{r_p}^{\infty} \left(\frac{d\phi_\theta}{dr} \right)^2 r dr \\
\eta_3 &= \int_{r_p}^{\infty} \phi_r \left(\frac{d\phi_r}{dr} \right) dr & \eta_4 &= \int_{r_p}^{\infty} \phi_\theta \left(\frac{d\phi_\theta}{dr} \right) dr \\
\eta_5 &= \int_{r_p}^{\infty} \phi_\theta \left(\frac{d\phi_r}{dr} \right) dr & \eta_6 &= \int_{r_p}^{\infty} \phi_r \left(\frac{d\phi_\theta}{dr} \right) dr \\
\eta_7 &= \int_{r_p}^{\infty} \frac{\phi_r^2}{r} dr & \eta_8 &= \int_{r_p}^{\infty} \frac{\phi_\theta^2}{r} dr \\
\eta_9 &= \int_{r_p}^{\infty} \frac{\phi_r \phi_\theta}{r} dr
\end{aligned} \tag{16}$$

The differential equations to calculate soil displacement shape functions $\phi_r(r)$ and $\phi_\theta(r)$ are obtained by collecting the terms containing $\delta\phi_r$, and $\delta\phi_\theta$ and equating each to zero. The coupled differential equations describing ϕ_r and ϕ_θ are:

$$\frac{d^2\phi_r}{dr^2} + \frac{1}{r} \frac{d\phi_r}{dr} - \left(\left(\frac{\gamma_1}{r} \right)^2 + \left(\frac{\gamma_2}{r_p} \right)^2 \right) \phi_r = \frac{\gamma_3^2}{r} \frac{d\phi_\theta}{dr} - \left(\frac{\gamma_1}{r} \right)^2 \phi_\theta \tag{17}$$

$$\frac{d^2\phi_\theta}{dr^2} + \frac{1}{r} \frac{d\phi_\theta}{dr} - \left(\left(\frac{\gamma_4}{r} \right)^2 + \left(\frac{\gamma_5}{r_p} \right)^2 \right) \phi_\theta = -\frac{\gamma_6^2}{r} \frac{d\phi_r}{dr} - \left(\frac{\gamma_4}{r} \right)^2 \phi_r \tag{18}$$

Equations (17) and (18) are subjected to boundary conditions $\phi_r = \phi_\theta = 1$ at $r = r_p$ and $\phi_r = \phi_\theta = 0$ at $r \rightarrow \infty$. The parameters γ_1 , γ_3 , γ_4 , and γ_6 in equations (17) and (18) are constants depending on soil properties and γ_2 and γ_5 depend on $w(z,t)$ at any given time and depth. These parameters are defined as:

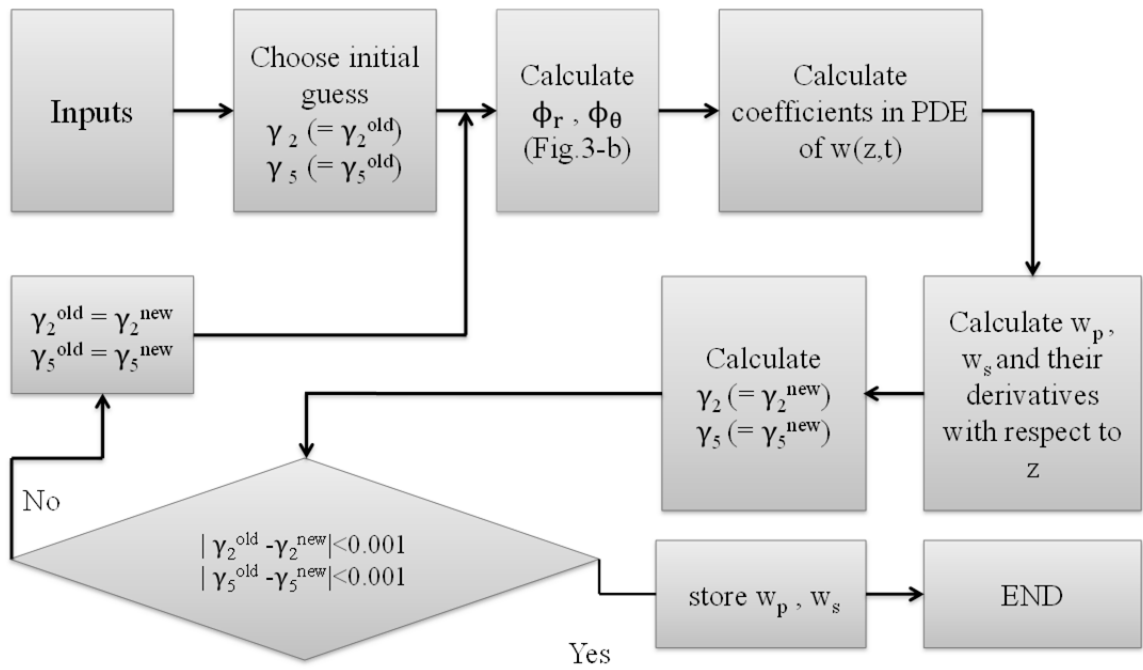
$$\begin{aligned}
\gamma_1^2 &= \frac{m_4}{m_1} = 1 + \frac{G}{\lambda + 2G} & \left(\frac{\gamma_2}{r_p} \right)^2 &= \frac{n - L}{m_1} \\
\gamma_3^2 &= \frac{m_2 + m_3}{m_1} = \frac{\lambda + G}{\lambda + 2G} & \gamma_4^2 &= \frac{m_4}{m_2} = 3 + \frac{\lambda}{G} \\
\left(\frac{\gamma_5}{r_p} \right)^2 &= \frac{n - L}{m_2} & \gamma_6^2 &= \frac{m_2 + m_3}{m_2} = 1 + \frac{\lambda}{G}
\end{aligned} \tag{19}$$

where:

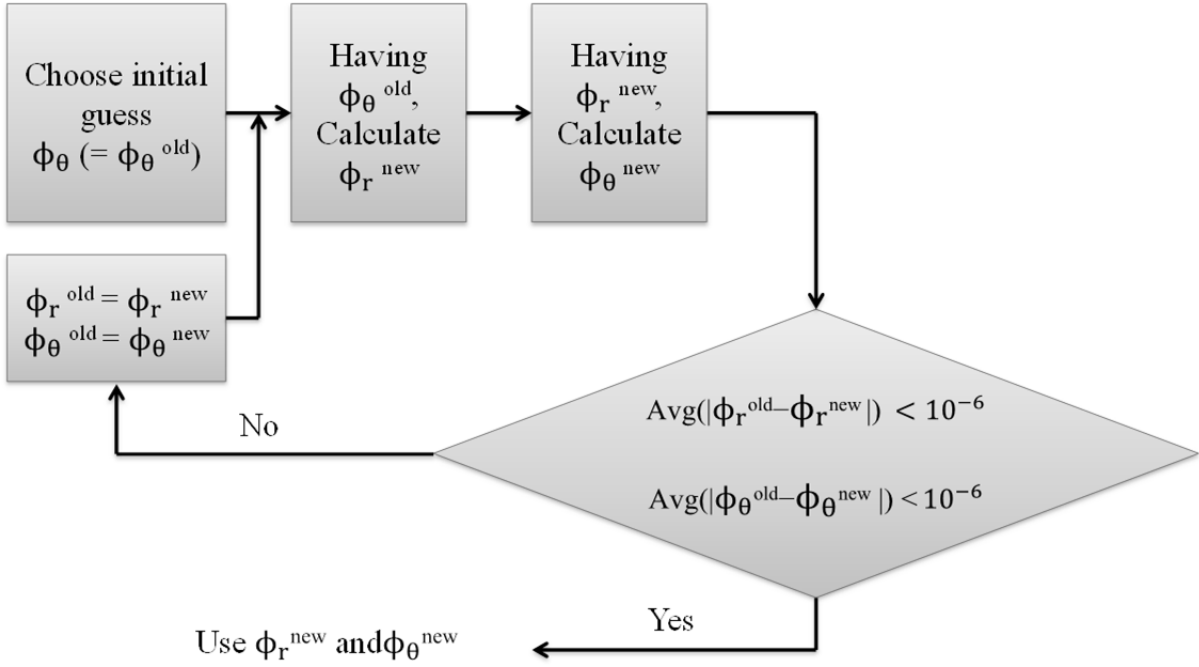
$$\begin{aligned}
 m_1 &= (\lambda + 2G) \int_0^\infty w^2 dz & m_2 &= G \int_0^\infty w^2 dz \\
 m_3 &= \lambda \int_0^\infty w^2 dz & m_4 &= (\lambda + 3G) \int_0^\infty w^2 dz \\
 n &= G \int_0^\infty \left(\frac{\partial w}{\partial z}\right)^2 dz & L &= \rho_s \int_0^\infty \left(\frac{\partial w}{\partial t}\right)^2 dz
 \end{aligned} \tag{20}$$

Solution algorithm

In order to obtain pile deflection as a function of depth and time, equation (10) should be solved. However, solution of equation (10) needs equation (11) to be solved first in order to satisfy boundary condition specified in equation (13a). Moreover, the coefficients k , M_1 , M_2 , τ and τ_s in equations (10) and (11) depend on ϕ_r and ϕ_θ , which are not known a priori. ϕ_r and ϕ_θ , on the other hand, are dependent on $w(z,t)$ and its derivatives through the parameters γ_2 and γ_5 (see equations 17, 18, and 19). Therefore, an iterative algorithm is necessary to solve the problem. Note that equations (17) and (18) are interdependent and should be solved simultaneously. So an iterative solution procedure is also warranted in order to quantify soil displacement shape functions. The flow chart presented in Fig. 3 shows the iterative solution steps.



(a)



(b)

Fig. 3. Solution flow chart: (a) for finding $w(z,t)$, (b) for finding $\phi_r(r)$ and $\phi_\theta(r)$

Solution for a specific case – undamped pile-soil system under steady state harmonic loading

The analytical framework outlined in the previous sections is used to solve for a specific case of undamped pile-soil system (i.e., $c=0$) subjected to steady state harmonic loading. The harmonic loading functions considered for this case are:

$$F(t) = F_0 e^{i\Omega t} \quad (21a)$$

$$M(t) = M_0 e^{i\Omega t} \quad (21b)$$

where Ω is the circular loading frequency and F_0 and M_0 are the amplitudes of the lateral load $F(t)$ and the moment $M(t)$, respectively. Pile and soil displacement are assumed to be in-phase with the loading function. Therefore, the motion of the pile and the soil column beneath it will be in the form of:

$$w(z, t) = \begin{cases} w_p(z) e^{i\Omega t} & , \quad 0 \leq z \leq L_p \\ w_s(z) e^{i\Omega t} & , \quad z \geq L_p \end{cases} \quad (22)$$

where $w_p(z)$ is the amplitude of the pile displacement, and $w_s(z)$ is the displacement amplitude for the soil column just beneath the pile. Substitution of equations (21) and (22) into equations (10) and (11) yields:

- *Differential equations*

$$E_p I_p \frac{d^4 w_p}{dz^4} - 2\tau \frac{d^2 w_p}{dz^2} + (k - M_1 \Omega^2) w_p = 0 \quad \text{for } 0 \leq z \leq L_p \quad (23)$$

$$-2\tau_s \frac{d^2 w_s}{dz^2} + (k - M_2 \Omega^2) w_s = 0 \quad \text{for } z \geq L_p \quad (24)$$

- *Boundary conditions*

At ground surface (i.e. $z = 0$):

$$E_p I_p \frac{d^3 w_p}{dz^3} - 2\tau \frac{dw_p}{dz} = F_0 \quad (25a)$$

$$E_p I_p \frac{d^2 w_p}{dz^2} = M_0 \quad (25b)$$

At pile base (i.e. $z = L_p$):

$$E_p I_p \frac{d^3 w_p}{dz^3} - 2\tau \frac{dw_p}{dz} + 2\tau_s \frac{dw_s}{dz} = 0 \quad (26a)$$

$$E_p I_p \frac{d^2 w_p}{dz^2} = 0 \quad (26b)$$

At the interface of soil and pile (i.e. $z = L_p$):

$$w_s = w_p \quad (27a)$$

At a point far below the pile; i.e., for $z \rightarrow \infty$

$$w_s = 0 \quad (27b)$$

The solution of equation (24) with boundary conditions expressed through equations (27a) and (27b) is given by:

$$w_s(z) = w_p(L_p) e^{-(z-L_p)\sqrt{\frac{k-M_2\Omega^2}{2\tau_s}}} \quad (28)$$

Equation (28) is used in equation (26a) to obtain the pile deflection.

Analytical Solution for Pile Deflection

The general solution of equation (23) can be written as:

$$w_p(z) = C_1 w_{p1} + C_2 w_{p2} + C_3 w_{p3} + C_4 w_{p4} \quad (29)$$

where w_{p1} , w_{p2} , w_{p3} , and w_{p4} are individual solutions of the fourth order differential equation and C_1 , C_2 , C_3 , and C_4 are integration constants. w_{p1} , w_{p2} , w_{p3} , and w_{p4} are trigonometric or hyperbolic functions arising in the solution of linear ordinary differential equations. Finding the individual solutions using Table 1, and then applying the boundary conditions specified in

equations (25) and (26) into equation (29), the integration constants, C_1 , C_2 , C_3 , and C_4 , can be determined. Equation (23) can be rearranged as:

$$\frac{d^4 w_p}{dz^4} - 2B \frac{d^2 w_p}{dz^2} + A w_p = 0 \quad (30)$$

where the two parameters A and B are expressed as:

$$A = \frac{k - M_1 \Omega^2}{E_p I_p} \quad (31a)$$

$$B^2 = \left(\frac{\tau}{E_p I_p} \right)^2 \quad (31b)$$

Based on the relative magnitude of A and B^2 , two cases are considered here. For each case, two other parameters, a and b, are defined and those are used in finding the individual solutions of the differential equation:

Case 1: $A > B^2$

$$a = \sqrt{\frac{1}{2}(\sqrt{A} + B)} \quad (32a)$$

$$b = \sqrt{\frac{1}{2}(\sqrt{A} - B)} \quad (32b)$$

Case 2: $A < B^2$

$$a = \sqrt{B + \sqrt{B^2 - A}} \quad (33a)$$

$$b = \sqrt{B - \sqrt{B^2 - A}} \quad (33b)$$

The individual solutions of equation (23), represented through equation (30), and their derivatives are outlined in Table 1. However, soil displacement shape functions must be quantified first to calculate individual solutions w_{p1} through w_{p4} .

Table 1 Individual solutions for pile displacement in equation 29

$B^2 < A$				
Individual solutions	Functions and their derivatives			
	w_p	w_p'	w_p''	w_p'''
w_{p1}	$\sinh az \cosh bz$	$aw_{p2} - bw_{p4}$	$(a^2 - b^2)w_{p1} - 2ab w_{p3}$	$a(a^2 - 3b^2)w_{p2} + b(b^2 - 3a^2)w_{p4}$
w_{p2}	$\cosh az \cosh bz$	$aw_{p1} - bw_{p3}$	$(a^2 - b^2)w_{p2} - 2ab w_{p4}$	$a(a^2 - 3b^2)w_{p1} + b(b^2 - 3a^2)w_{p3}$
w_{p3}	$\cosh az \sinh bz$	$aw_{p4} + bw_{p2}$	$(a^2 - b^2)w_{p3} + 2ab w_{p1}$	$a(a^2 - 3b^2)w_{p4} - b(b^2 - 3a^2)w_{p2}$
w_{p4}	$\sinh az \sinh bz$	$aw_{p3} + bw_{p1}$	$(a^2 - b^2)w_{p4} + 2ab w_{p2}$	$a(a^2 - 3b^2)w_{p3} - b(b^2 - 3a^2)w_{p1}$
$A < B^2$				
Individual solutions	Functions and their derivatives			
	w_p	w_p'	w_p''	w_p'''
w_{p1}	$\sinh az$	aw_{p2}	a^2w_{p1}	a^3w_{p2}
w_{p2}	$\cosh az$	aw_{p1}	a^2w_{p2}	a^3w_{p1}
w_{p3}	$\sinh bz$	bw_{p4}	b^2w_{p3}	b^3w_{p4}
w_{p4}	$\cosh bz$	bw_{p3}	a^2w_{p4}	b^3w_{p3}

Finite Difference Formulation for Soil Displacement Shape Functions

The differential equations for ϕ_r and ϕ_θ (equations 17 and 18) are solved numerically using finite difference formulation. Using the central-difference scheme, finite difference forms of equations (17) and (18) can be written as:

$$\frac{\Phi_r^{j+1} - 2\Phi_r^j + \Phi_r^{j-1}}{\Delta r^2} + \frac{1}{r_j} \frac{\Phi_r^{j+1} - \Phi_r^{j-1}}{2\Delta r} - \left[\left(\frac{\gamma_1}{r_j} \right)^2 + \left(\frac{\gamma_2}{r_p} \right)^2 \right] \Phi_r^j = \frac{\gamma_3^2}{r_j} \frac{\Phi_\theta^{j+1} - \Phi_\theta^{j-1}}{2\Delta r} - \left(\frac{\gamma_1}{r_j} \right)^2 \Phi_\theta^j \quad (34)$$

$$\frac{\Phi_\theta^{j+1} - 2\Phi_\theta^j + \Phi_\theta^{j-1}}{\Delta r^2} + \frac{1}{r_j} \frac{\Phi_\theta^{j+1} - \Phi_\theta^{j-1}}{2\Delta r} - \left[\left(\frac{\gamma_4}{r_j} \right)^2 + \left(\frac{\gamma_5}{r_p} \right)^2 \right] \Phi_\theta^j = -\frac{\gamma_6^2}{r_j} \frac{\Phi_r^{j+1} - \Phi_r^{j-1}}{2\Delta r} - \left(\frac{\gamma_4}{r_j} \right)^2 \Phi_r^j \quad (35)$$

where Δr is discretization length and j is the nodal index (Fig. 4).

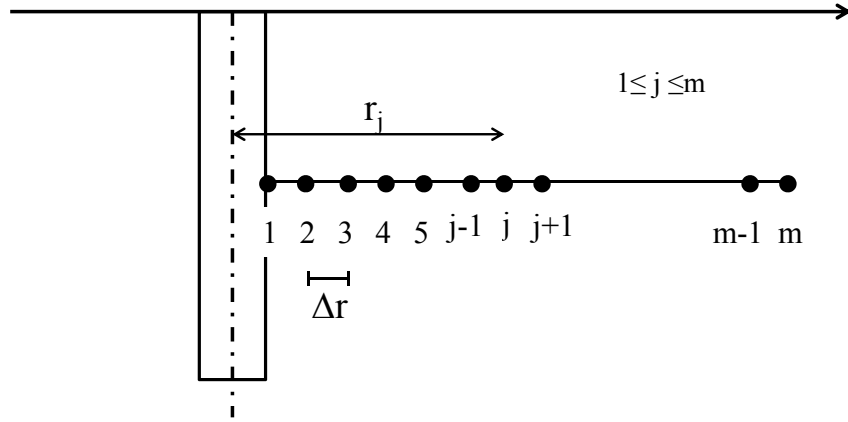


Figure 4 Finite difference discretization in radial direction

Δr should be sufficiently small to maintain a satisfactory level of accuracy and the total number of nodes m should be sufficiently large to adequately model the infinite domain in the radial direction. After applying the boundary conditions, equation (34) and (35) can be written in matrix form as:

$$[K^{\phi_r}]_{m \times m} [\phi_r]_{m \times 1} = [F^{\phi_r}]_{m \times 1} \quad (36a)$$

$$[K^{\phi_\theta}]_{m \times m} [\phi_\theta]_{m \times 1} = [F^{\phi_\theta}]_{m \times 1} \quad (36b)$$

In equation (36), $[K^{\phi_r}]$ and $[K^{\phi_\theta}]$ are tri-diagonal matrices with elements $K_{ji}^{\phi_r}$ and $K_{ji}^{\phi_\theta}$

$$K_{ji}^{\phi_r} = \begin{cases} 1 & , i = j = 1 \text{ or } m \\ \frac{1}{\Delta r^2} - \frac{1}{2r_j \Delta r} & , i = j - 1 \text{ and } j \neq 2 \\ -\frac{2}{\Delta r^2} - \left[\left(\frac{\gamma_1}{r_j} \right)^2 + \left(\frac{\gamma_2}{r_p} \right)^2 \right] & , 2 \leq i = j \leq m - 1 \\ \frac{1}{\Delta r^2} + \frac{1}{2r_j \Delta r} & , i = j + 1 \text{ and } j \neq m - 1 \\ 0 & , \text{others} \end{cases} \quad (37a)$$

$$K_{ji}^{\phi_\theta} = \begin{cases} 1 & , i = j = 1 \text{ or } m \\ \frac{1}{\Delta r^2} - \frac{1}{2r_j \Delta r} & , i = j - 1 \text{ and } j \neq 2 \\ -\frac{2}{\Delta r^2} - \left[\left(\frac{\gamma_4}{r_j} \right)^2 + \left(\frac{\gamma_5}{r_p} \right)^2 \right] & , 2 \leq i = j \leq m - 1 \\ \frac{1}{\Delta r^2} + \frac{1}{2r_j \Delta r} & , i = j + 1 \text{ and } j \neq m - 1 \\ 0 & , \text{others} \end{cases} \quad (37b)$$

and the elements of $[F^{\phi_r}]_{m \times 1}$ and $[F^{\phi_\theta}]_{m \times 1}$ are:

$$F_j^{\phi_r} = \begin{cases} 1 & , j = 1 \\ -\frac{1}{\Delta r^2} + \frac{1}{2r_2 \Delta r} + \frac{\gamma_3^2 \phi_\theta^{(3)} - 1}{r_2 \cdot 2 \Delta r} - \left(\frac{\gamma_1}{r_2} \right)^2 \phi_\theta^{(2)} & , j = 2 \\ \frac{\gamma_3^2 \phi_\theta^{j+1} - \phi_\theta^{j-1}}{r_j \cdot 2 \Delta r} - \left(\frac{\gamma_1}{r_j} \right)^2 \phi_\theta^j & , 3 \leq j \leq m - 2 \\ \frac{\gamma_3^2 \phi_\theta^{(m-2)} - \phi_\theta^{(m-1)}}{r_{m-1} \cdot 2 \Delta r} - \left(\frac{\gamma_1}{r_{m-1}} \right)^2 \phi_\theta^{(m-1)} & , j = m - 1 \\ 0 & , j = m \end{cases} \quad (38a)$$

$$F_j^{\phi_\theta} = \begin{cases} 1 & , j = 1 \\ -\frac{1}{\Delta r^2} + \frac{1}{2r_2 \Delta r} - \frac{\gamma_6^2 \phi_r^{(3)} - 1}{r_2 \cdot 2 \Delta r} - \left(\frac{\gamma_4}{r_2} \right)^2 \phi_r^{(2)} & , j = 1 \\ -\frac{\gamma_6^2 \phi_r^{j+1} - \phi_r^{j-1}}{r_j \cdot 2 \Delta r} - \left(\frac{\gamma_4}{r_j} \right)^2 \phi_r^j & , 3 \leq j \leq m - 2 \\ -\frac{\gamma_6^2 \phi_r^{(m-2)} - \phi_r^{(m-1)}}{r_{m-1} \cdot 2 \Delta r} - \left(\frac{\gamma_4}{r_{m-1}} \right)^2 \phi_r^{(m-1)} & , j = m - 1 \\ 0 & , j = m \end{cases} \quad (38b)$$

Since, the right-hand side vectors $[F^{\phi_r}]_{m \times 1}$ and $[F^{\phi_\theta}]_{m \times 1}$ in equation (36) have elements containing the unknown ϕ_r and ϕ_θ , iterative procedures should be followed to obtain their values as illustrated in solution flowchart (Fig.3b). A MATLAB code is developed to handle the iterative solution procedure described herein. Note that the CPU runtime of the MATLAB code (run on a core-i5 processor with 8 GB RAM) is approximately 100 s for the example cases presented in this report.

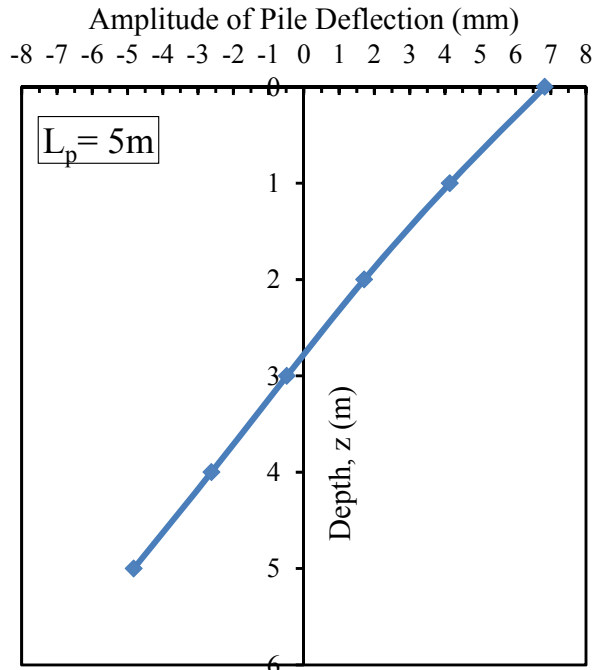
Results and Discussions

The application of the developed analysis methodology is demonstrated using an example problem with input parameters listed in Table 2.

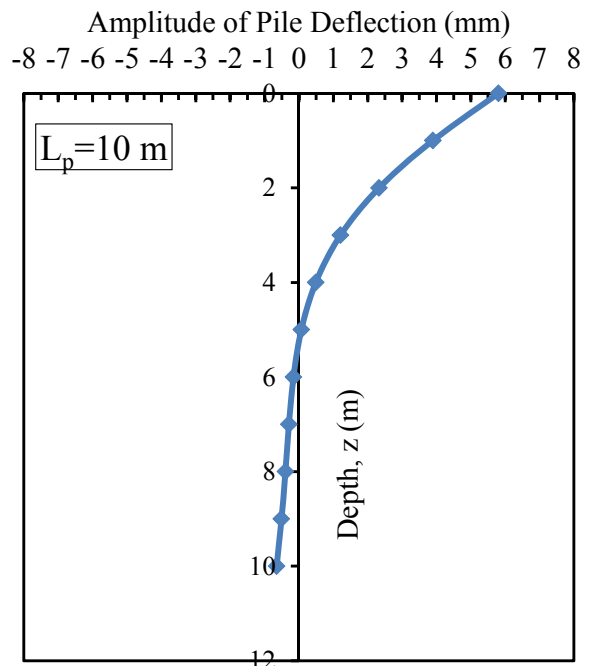
Table 2- Input parameters used in the analysis of sample problem

Pile Geometry	Radius, r_p (mm)	0.5
	Length, L_p (m)	5, 10, 15, 20
Material Properties for Pile	Modulus of Elasticity, E_p (Gpa)	25
	Density, ρ_p (kg/m ³)	2400
Material Properties for Soil	Modulus of Elasticity, E_s (Mpa)	25
	Poisson Ratio, ν_s	0.3
	Density, ρ_s (kg/m ³)	1500
Force	Amplitude, F_0 (kN)	1000
	Circular Frequency, Ω (rad/s)	10

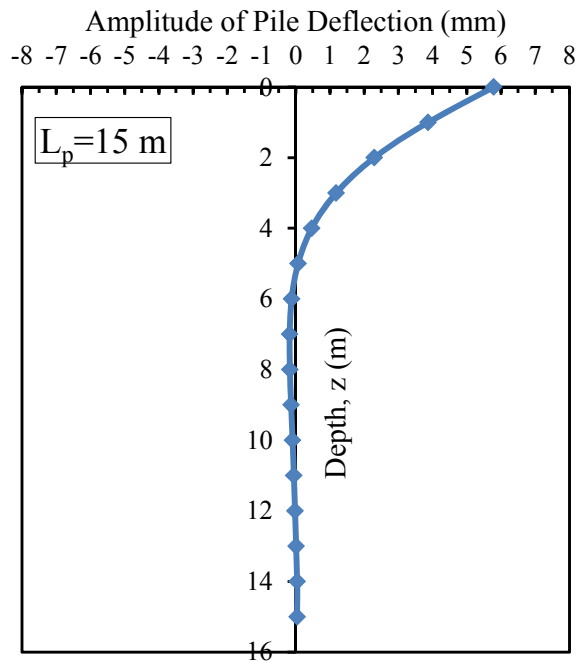
The effects of pile length L_p and pile-to-soil stiffness ratio are also investigated. Fig. 5 shows the amplitude of pile deflection, $w_p(z)$, for different pile lengths (= 5m, 10m, 15m, and 20m). For pile length $L_p = 5$ m, a rigid body rotation that signifies short-pile response under lateral loading, is observed. A transition behavior is observed for $L_p = 10$ m and the pile behaves as a long-pile for $L_p = 15$ and 20m. Figure 6 shows, at some selected time instants, the variation of pile deflection with depth.



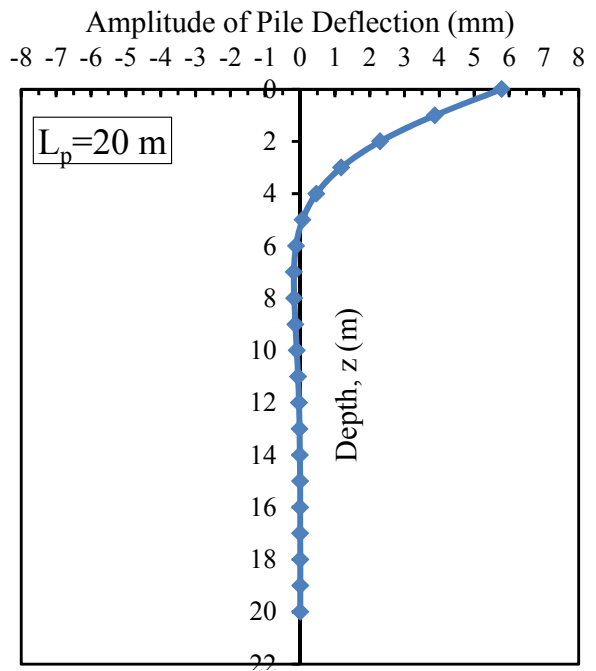
a)



b)



c)



d)

Fig.5. Amplitude of pile deflection along the pile length ($w_p(z)$)

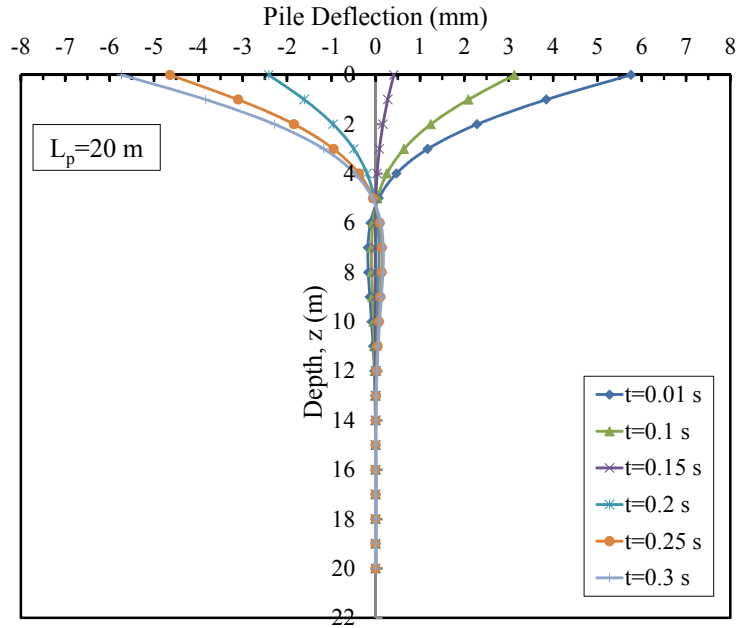
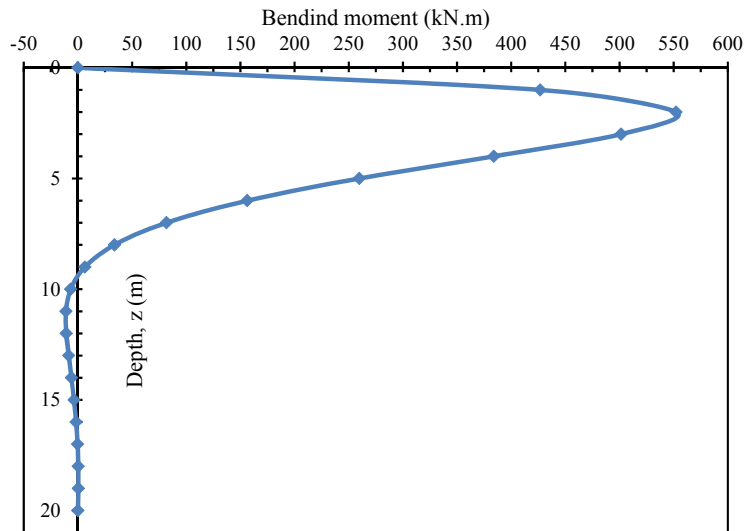
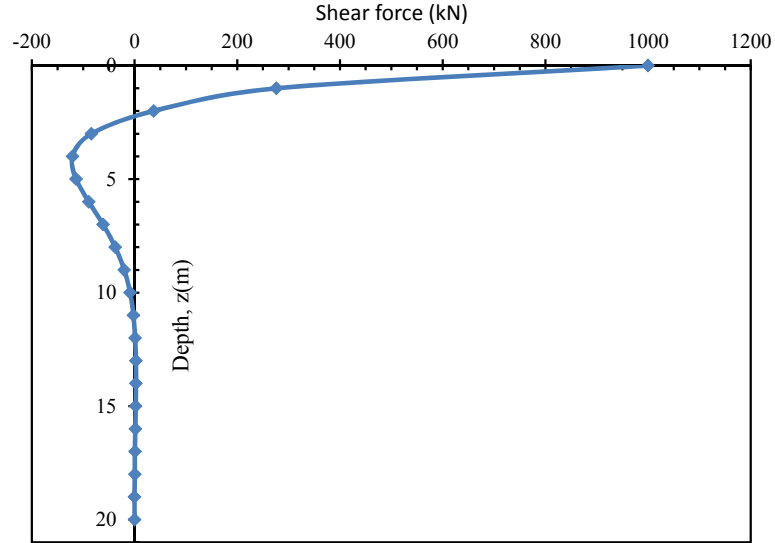


Fig.6. Pile Deflection at different time instants

The bending moment and shear force at different pile cross-sections are important design parameters for laterally loaded piles. Figure 7 shows the variation of bending moment and shear force with along the length of a 10-m-long pile. The maximum bending moment occurs at a depth of 2 m ($= L_p/10$) from the pile head and the maximum shear force occurs at the pile head.



7(a)



7(b).

Fig.7. (a) Bending moment and (b) Shear force diagram along the pile length

A parametric study is done to investigate the effects of parameters L_p/r_p (i.e., slenderness ratio of the pile) and E_p/E_s (i.e., pile-soil modulus ratio) on pile behavior under harmonic lateral loading. Figure 8 shows that lateral displacement of pile base is more sensitive to change in pile slenderness ratio L_p/r_p when compared to pile head displacement. Both pile head and base displacements decrease with increase in L_p/r_p ; nonetheless, they become insensitive to the change in slenderness ratio for $L_p/r_p \geq 25$.

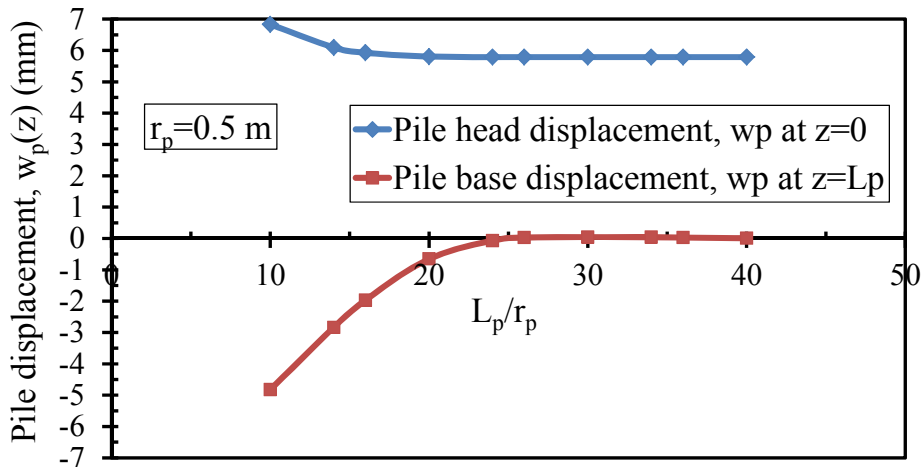


Fig.8. Effect of pile slenderness ratio L_p/r_p on pile head and base displacements

For a long pile ($L_p = 25$ m), the ratio E_p/E_s of elastic modulus of deformation for pile and soil significantly affects the displacement at the pile head; pile head displacement appears to be linearly proportional with E_p/E_s . The displacement at pile base also increases as the ratio E_p/E_s increases (or E_s decreases); however, the relationship between these two parameters is not linear (Fig. 9).

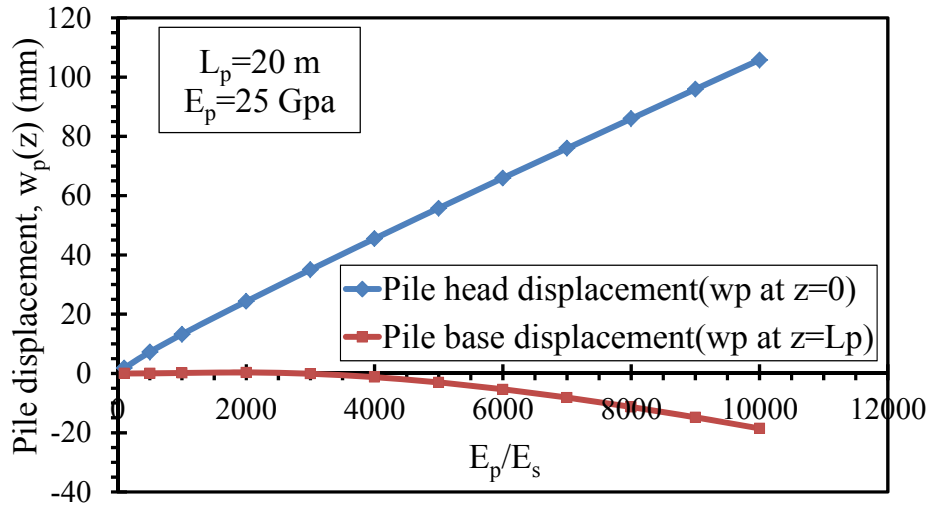


Fig. 9. Effect of E_p/E_s on the displacement of the pile at the head and the bottom

The variations of soil displacement shape functions, ϕ_r and ϕ_θ , with radial distance from the pile are presented in Figure 10. The slope of decay in the soil displacement shape function is larger in tangential direction than that in the radial direction. Figures 11 and 12 shows soil displacements u_r and u_θ recorded at different depths z and at different angular coordinates θ ($= 0, \frac{\pi}{6}, \frac{\pi}{3}, \frac{\pi}{2}$) with respect to the direction of the applied force. Note that $u_r = u_\theta = 0$ for $\theta = 0$ and $\theta = \frac{\pi}{2}$, which directly follows the assumption of no separation between pile and soil surrounding it (an assumption necessary for the present analytical continuum-based approach). Figure 13 demonstrates the effects of radial distance and angle with respect to the direction of the applied load on the radial and tangential displacement at any point (for depth $z = 0.5$ m).

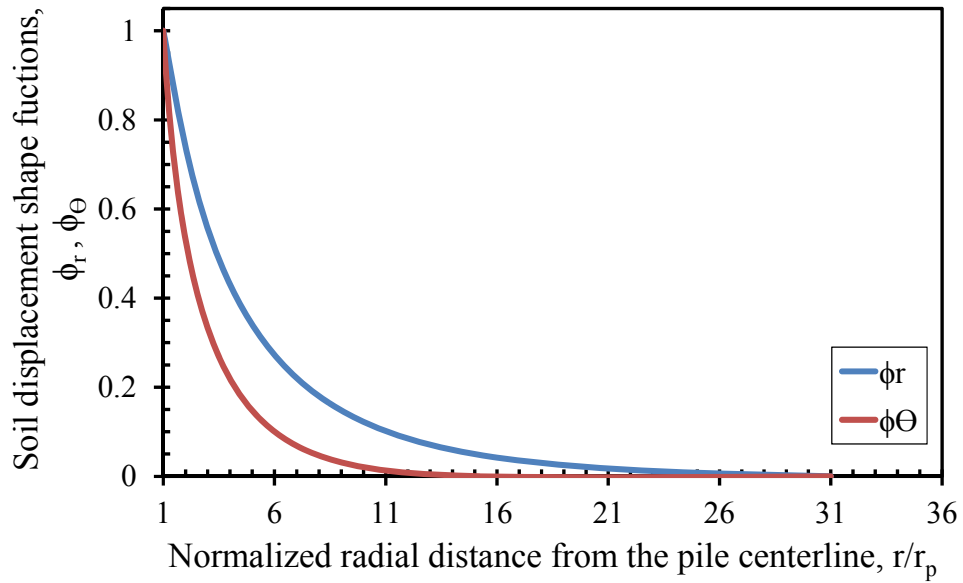
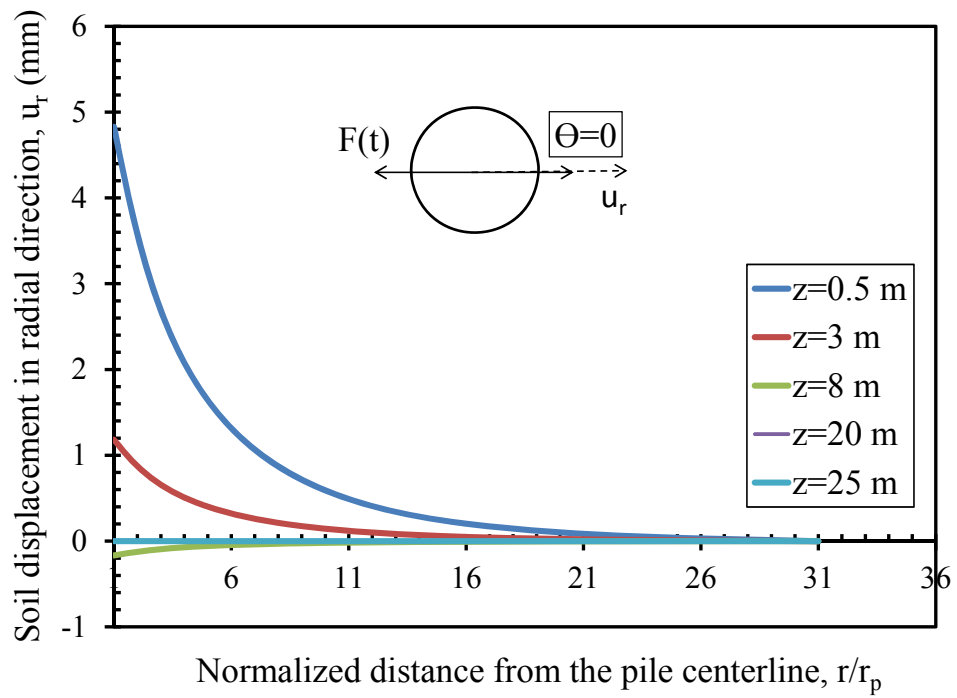
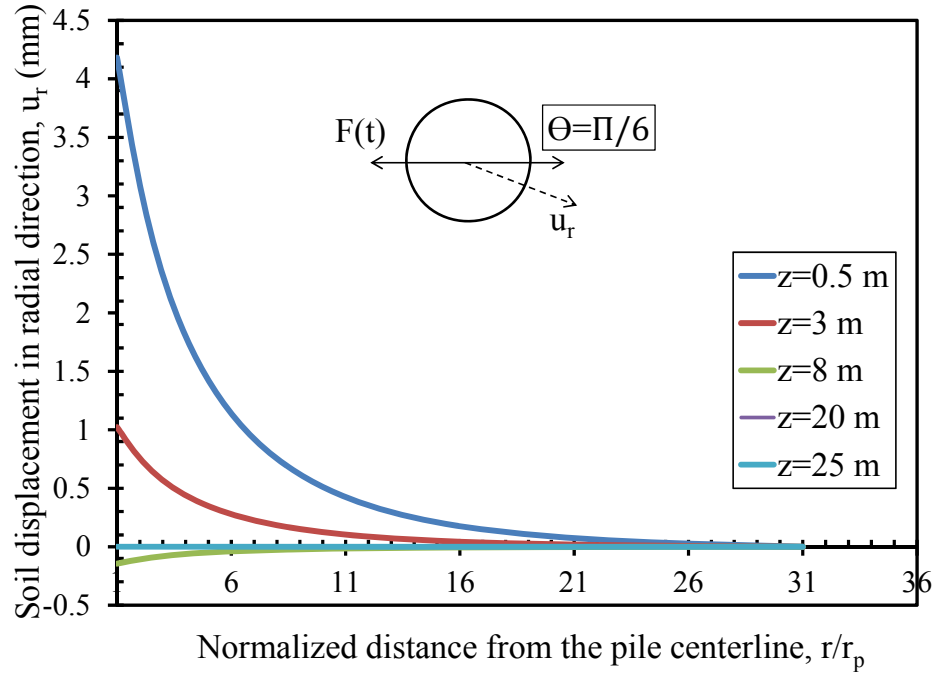


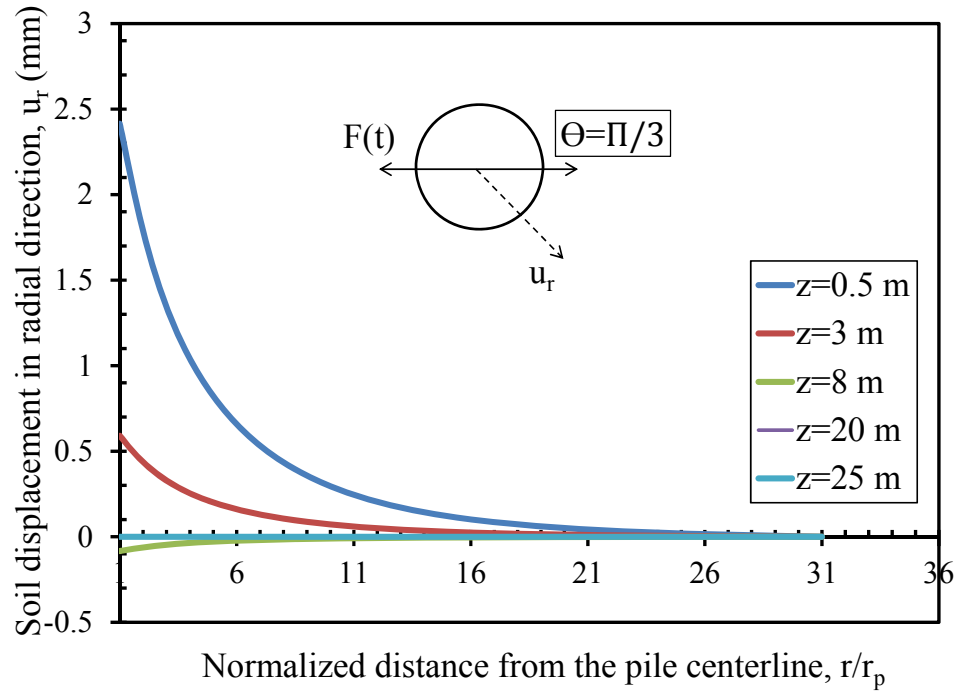
Fig. 10. variation of soil displacement shape functions, $\phi_r(r)$ and $\phi_\theta(r)$



11(a)

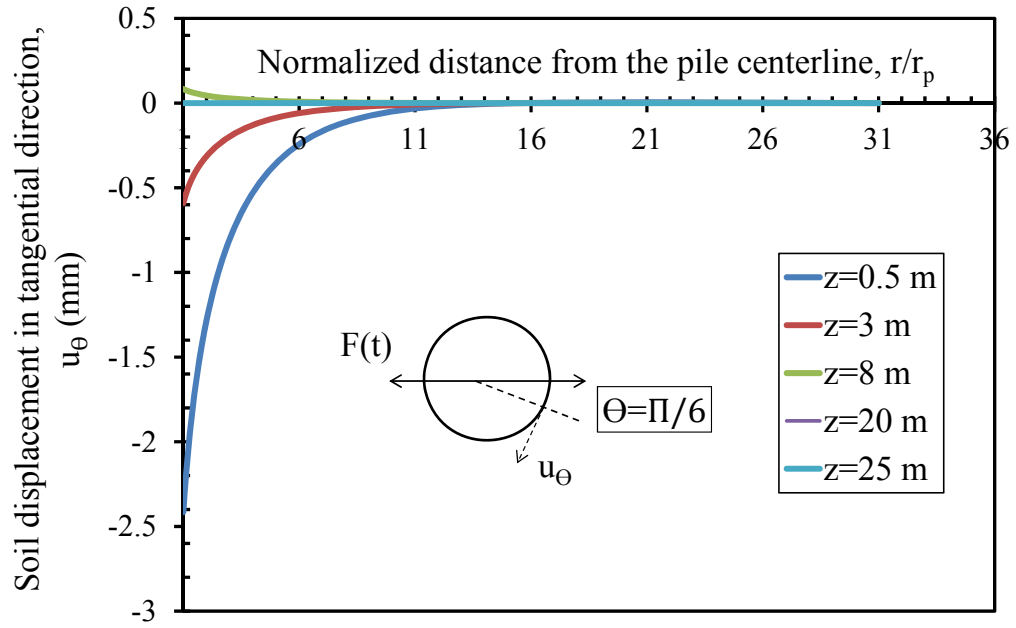


11(b)

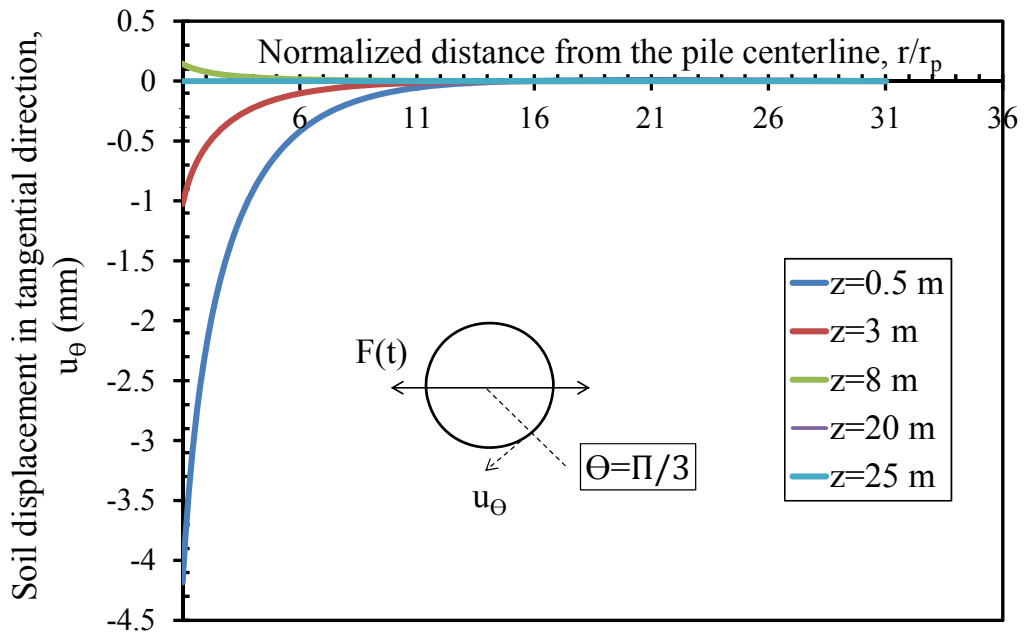


11(c)

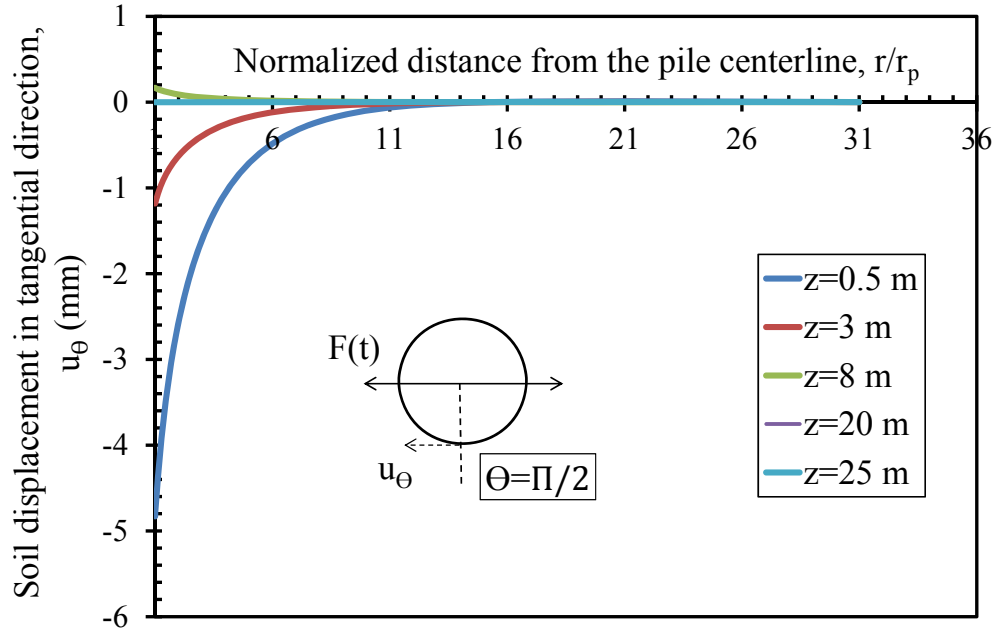
Fig.11. Soil displacement in radial direction at the angle of (a) $\theta = 0$, (b) $\theta = \frac{\pi}{6}$, (c) $\theta = \frac{\pi}{3}$ with respect to the direction of the applied force, at different depth, ($L_p=20$ m)



12(a)

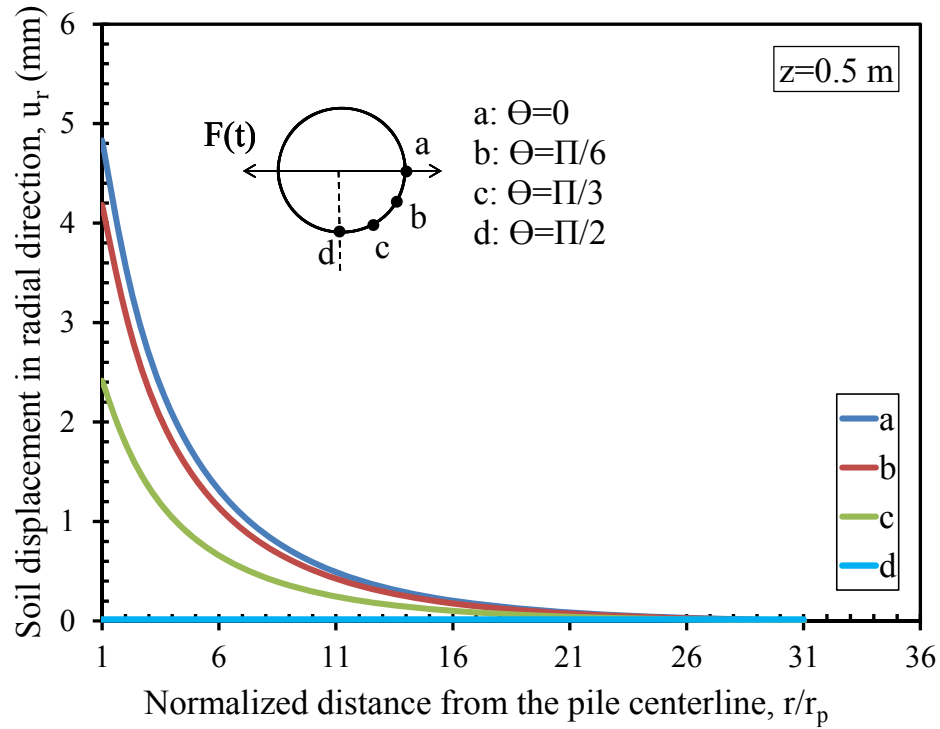


12(b)

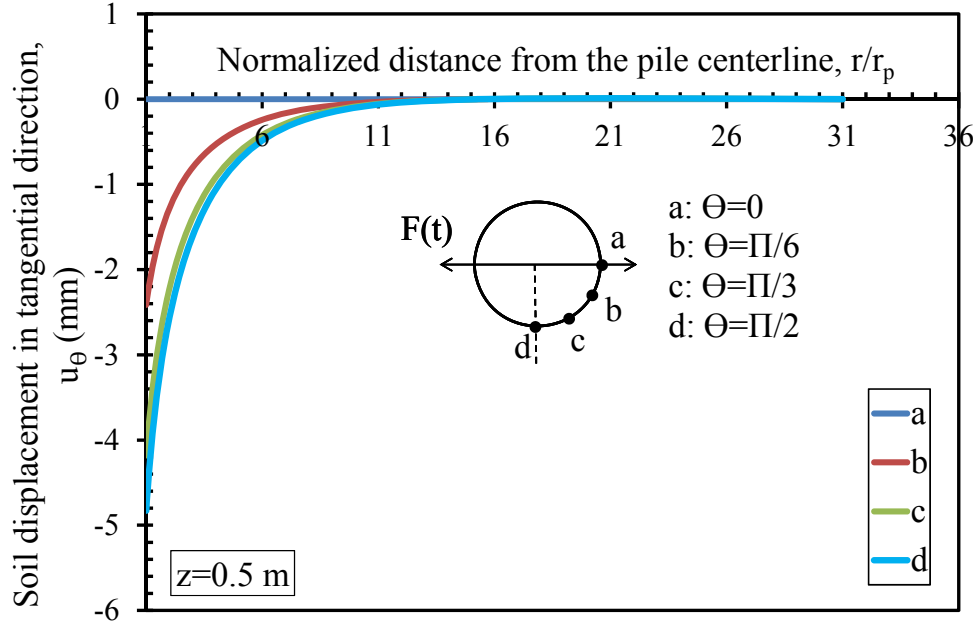


12(c)

Fig.12. Soil displacement in tangential direction at the angle of (a) $\theta = \frac{\pi}{6}$, (b) $\theta = \frac{\pi}{3}$, (c) $\theta = \frac{\pi}{2}$ with respect to the direction of the applied force, at different depth, ($L_p=20$ m)



13(a)



13(b)

Fig.13. Variation of soil displacement (for $L_p=20$ m and $z=0.5$ m) at various locations within the domain surrounding the pile (a) radial displacement u_r and (b) tangential displacement u_θ

Summary and Conclusions

A semi-analytical continuum-based approach is developed for predicting response of a single pile subjected to dynamic lateral loading. Soil surrounding the pile is considered to be elastic, homogeneous and isotropic. A MATLAB code is developed to perform analysis following the proposed framework. It appears that the developed semi-analytical framework is computationally efficient (much so when compared to 3D FEAs). Although results show promise of the analysis methodology presented in this report, accuracy of such results needs further verification using real-life data and/or conventional three-dimensional finite element analyses.

References

- Basu, D., Salgado, R., Prezzi, M., 2009, A Continuum-Based Model for Analysis of Laterally Loaded Piles in Layered Soils, *Geotechnique* 59(2), 127-140
- Bentley, K. J., El Naggar, M. H., 2000, Numerical Analysis of Kinematic response of Single Piles, *Can. Geotech. J.*, 37(6), 1368-1382
- Das, Y. C., Sargand, S. M., 1999, Forced Vibration of Laterally Loaded Piles, *international journal of solids and structures*, 36, 4975-4989
- El naggar, M. H., Bentley, K. J., 2000, Dynamic Analysis for Laterally Loaded Piles and Dynamic p-y Curves, *Can. Geotech. J.*, 37(6), 1166-1183
- Krishna, R., Gazetas, G., Velez, A., 1983, Static and Dynamic lateral deflection of piles in nonhomogeneous soil stratum, *Geotechnique*, 33(3), 307-326
- Kuhlemaier, R. L., 1979, Static and Dynamic laterally loaded floating piles, *J. Geotech. Engrg.*, 105(2) 289-304
- Maheshwari, B. K., Truman, K. Z., El Naggar, M. H., Gould, P. L., 2004, Three-Dimensional Finite Element Nonlinear Dynamic Analysis of Pile Groups for Lateral Transient and Seismic Excitations, *Can. Geotech. J.*, 41(1), 118-133
- Maheshwari, B. K., and Watanabe, H., 2006, Nonlinear Dynamic Behavior of Pile Foundations: Effects of Separation at Soil-Pile Interface, *Soils Found.*, 46(4), pp. 437-448
- Matlock, H., Foo, S. H., Bryant, L. L. 1978, Simulation of Lateral pile Behavior, *Proc. Earthquake Engrg. And Soil Dyn. ASCE*, Pasadena, California, July, 600-619
- Nogami, T., Konagai, K., 1988, Time-Domain Flexural Response of Dynamically Loaded Single Piles, *Engrg. Mech. ASCE*, 114(9), 1512-1525.
- Nogami, T., Otani, J., Konagai, K., Chen, H.L., 1991, Nonlinear Soil-Pile Interaction Model for Dynamic Lateral Motion, *J. Geotech. Engrg, ASCE*
- Novak, M., 1974, Dynamic Stiffness and Damping of Soils, *J. Can. Geotech. Engrg. NRC of Canada*, 11(5), 574-698.
- Velez, A., Gazetas, G., Krishna, R., 1983, Lateral Dynamic Response of Constrained-Head Piles, *ASCE J. Geotech. Engrg.*, 109(8), 1063-1081